FABRICATION OF FLUORINATED GRAPHENE BASED ARAMID NANOFIBERS FILMS WITH EXCELLENT THERMAL CONDUCTIVITY AND MECHANICAL PROPERTIES

Minh-Canh Vu[1]*, Minh-Sang Tran[2], Quang Bang Tao[2], Van-Thanh Hoang[2]

[1]The University of Danang – Advanced Institute of Science and Technology, Danang, Vietnam
[2]The University of Danang – University of Science and Technology, Danang, Vietnam

*Corresponding authors: vmcanh@aist.udn.vn

(Received: October 24, 2023; Revised: December 12, 2023; Accepted: December 13, 2023)

Abstract - The rapid advancement of technology has spurred the development of a wide range of sophisticated electronic devices leading to an increasing demand for the utilization of thermoconductive materials to address thermal management. However, most of the available thermoconductive materials possess inadequate mechanical properties and low resistance to temperatures. To address this limitation, this study focuses on fabricating the thermoconductive films using aramid nanofiber (ANF) as strengthening components and fluorinated graphene (FG) as a thermoconductive filler. The films are prepared through the simple vacuum filtration method. The obtained FG/ANF film with 40 wt% of FG reached the in-plane thermal conductivity of 9 W/mK. Additionally, the FG40/ANF film exhibits excellent mechanical properties, including a tensile strength exceeding 110 MPa and toughness greater than 7.2 MJ/m³. Given these remarkable characteristics, the FG/ANF film holds significant promise as a material for dissipating heat in electronic devices, particularly in applications that demand high mechanical performance and temperature stability.

Key words - Thermal conductivity; mechanical properties; fluorinated graphene (FG); aramid nanofiber (ANF); vacuum filtration

1. Introduction

Next-generation electronics are currently under development, with a focus on achieving high power, integrating multiple technologies, multitasking, and reducing size, aiming for thinner, lighter, and more compact designs [1, 2]. However, these advanced electronics generate more heat during operation. The accumulation of excessive heat significantly impacts device stability, lifespan, and poses potential fire and health hazards to users. Research indicates that a 1-2°C increase in a device's operating temperature can reduce its lifespan by 10-20% [3, 4]. To address these challenges, advanced thermally conductive materials with high thermal conductivity have become crucial.

One solution involves polymer composites mixed with thermally conductive fillers like graphene, carbon nanotubes, aluminum nitride, and nano boron nitride [5, 6]. Among these, graphene stands out due to its exceptional thermal conductivity (5300 W/mK) and mechanical properties [7]. For instance, Vu et al. reported that polymer composites with a 5 wt% fraction of functionalized graphene filler achieved a high thermal conductivity of0.6 W/mK [8]. Additionally, graphene nanoplatelet-based aramid nanofiber films exhibited a remarkable thermal conductivity of 68.2 W/mK [9]. However, these composites often possess high electrical conductivity due to graphene's inherent electrical properties, limiting their use in applications requiring electrical insulation.

Fluorinated graphene (FG), a derivative of graphene, has garnered attention for its high electrical resistivity, a result of structural changes during fluorination from sp^2 to sp^3 carbon-carbon bonds [10]. FG has demonstrated excellent insulating properties with resistivity exceeding 10^{12} Ω·cm [10]. Moreover, the theoretical thermal conductivity of FG reaches 1800 W/mK at 100% fluorination [11], addressing the electrical conductivity challenge while maintaining high thermal conductivity. Dineshkumar et al. reported the use of 3D FG-based epoxy composites for heat dissipation, achieving a thermal conductivity of 9.68 W/mK [12]. However, challenges persist in creating polymer composites with superior mechanical properties and thermal stability, particularly for aerospace and military applications.

In this study, we explored the fabrication of composite films combining one-dimensional aramid nanofibers (ANF) and two-dimensional fluorinated graphene (FG) using vacuum filtration. The FG/ANF films incorporate unidirectional aramid nanofibers for reinforcement and 2D FG nanosheets for thermal conductivity. ANF was chosen for its surface functional groups, enhancing heat transfer within the FG/ANF films, as well as its thermal stability and mechanical strength. The resulting FG/ANF films exhibited a well-aligned layered structure with uniform FG dispersion. The FG40/ANF film, with 40 wt% FG, achieved an outstanding in-plane thermal conductivity of 9.2 W/mK. Furthermore, the FG/ANF film demonstrated excellent thermal stability, maintaining consistent thermal conductivity up to 200°C. Notably, the FG40/ANF film exhibited high tensile strength (>110 MPa) and toughness (7.2 MJ/m³). With these remarkable properties, FG/ANF films have the potential to serve as excellent thermal management materials for high-power electronic systems and devices, contributing to scientific and technological advancements.

2. Materials and methods

2.1. Materials

Fluorinated graphite was provided by ACS Materials (USA), dimethylsulfoxide (DMSO) and potassium hydroxide (KOH) were purchased from Thermo Fisher (USA). Kevlar fibers were obtained from Dupont (USA). PTFE membrane (pore size of 0.45 μm) was received from

GVS S.p.A (Italy). All other solvents were received and used without purification.

2.2. Preparation of aramid nanofibers

Aramid nanofibers were prepared by the deprotonation of Kevlar fibers according to the scheme depicted in Figure 1 [13]. 0.9 g of KOH was first dissolved in a mixture of 192 ml DMSO and 8 ml H_2O. Then, 0.6 g of Kevlar fibers (cut into small segments of 5-10 cm) were added to the solution. The mixture in a beaker was stirred using a magnetic stirrer (at 500 rpm) in an oil bath at a temperature of 70°C for 4 hours to obtain a dark red solution of nano aramid fibers with a concentration of 3 mg/ml.

2.3. Preparation of fluorinated graphene

Fluorinated graphene was prepared from fluorinated graphite by the sonication method. 0.2 g of fluorinated graphite was dispersed in 100 ml of ethanol and followed to sonicate for 60 min. The obtained solution was under centrifuged at 1000 rpm for 5 min to remove the unexfloliated fluorinated graphite. The supernatant was collected and vacuum filtered to receive the wet FG which was then dried at 90°C for 12 hours to obtain FG powder.

2.4. Fabrication of FG/ANF films

Firstly, a certain amount of FG was added to 10 ml of ethanol solvent and stirred at 500 rpm for 15 min to ensure good dispersion of FG in ethanol. Meanwhile, a solution of ANF was taken in a beaker and then 10 ml of distilled water was added while stirring (at 500 rpm) for 5 min to wash the nano aramid fibers. The resulting mixture was then vacuum filtered to remove the washing solution, leaving the relatively moist filter residue. The filter residue was placed in 10 ml of ethanol and stirred at 500 rpm for 15 min to form ANF/ethanol solution. Then, ANF/ethanol solution was added to the beaker containing the initial FG/ethanol solution and stirred at 1000 rpm for 15 min to achieve uniform dispersion of FG in the ANF solution. Finally, the FG/ANF mixture was filtered through a polytetrafluoroethylene (PTFE) membrane to form the FG/ANF film. The filtered film was dried at a temperature of 90°C for 2 days. A series of FG/ANF films with different mass fractions of FG (20-60%) were prepared. For comparison, a pure ANF film was also fabricated.

2.5. Characterization

The morphology of the fillers was observed using a high-resolution field-emission scanning electron microscope (JEOL 7610F, JEOL, Japan). The X-ray diffractometer (XRD, D8 Advance, Bruker Co., USA) was used for the analysis of the crystalline structure of fluorinated graphene, employing CuK_α radiation with a wavelength (λ) of 1.5418 Å. The instrument operated at an accelerating voltage of 40 kV and an electron current of 40 mA. The scanning speed was set at 5°/min, ranging from 1° to 70°. Fourier transform infrared spectra (FT-IR) were conducted on a Nicolet IR 200 (Thermo Electron, Japan). Transmission electron microscope (TEM) was observed on a JEM-2100F (JEOL, Japan). The laser flash instrument (LFA 427, Netzsch) was utilized to determine the thermal diffusivity (α, cm^2/s) of the FG/ANF films in both in-plane and through-plane directions at various temperatures. The thermal conductivity (λ, W/mK) was calculated by multiplying the density (ρ, kg/cm^3) and specific heat (Cp, J/kgK). Mechanical strength of FG/ANF films was conducted on strips of the films with dimensions of 0.5 × 2.5 cm using a texture analyzer (SurTA 1A, Chemilab Co., Korea). The speed of the grip was controlled at 1 mm/s. The tensile toughness can be measured by the area under the stress/strain curve to fracture.

The sheet resistivity of the FG/ANF films was measured using the 4-probe method. The volume resistivity was determined by converting the sheet resistivity based on the thickness and contact area of the sample.

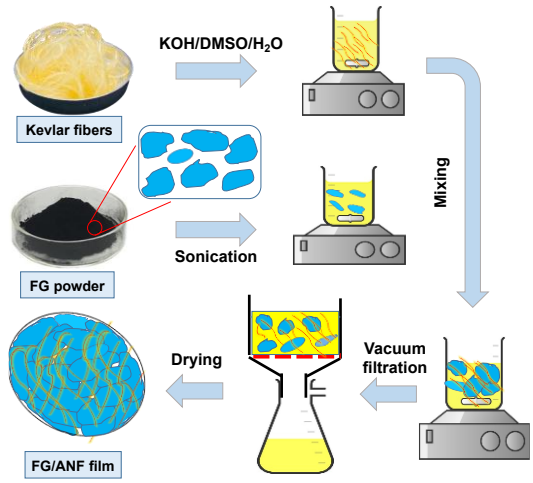

Figure 1. *Schematic illustration for the fabrication process of FG/ANF films*

3. Results and discussion

3.1. Morphology

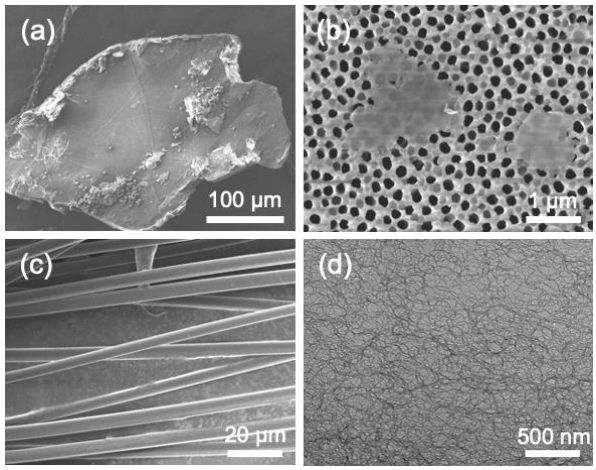

Figure 2. *SEM images of (a) fluorinated graphite, (b) FG, (c) Kevlar fibers and (d) TEM image of ANF.*

The fabrication process of fluorinated graphene (FG) involved exfoliating fluorinated graphite using the sonication method, as depicted in Figure 1. Initially, 200 mg of fluorinated graphite flakes were dispersed in 100 ml of ethanol and subjected to 4 hours of tip-sonication. Figure 2a displays an SEM image of a piece of fluorinated graphite with a lateral size of 200-300 µm and significant thickness. The resulting fluorinated graphene exhibited a well-defined sheet-like structure. After exfoliation, the FG nanosheet solution was

obtained through centrifugation and the collection of the supernatant. 1 ml of FG supernatant was deposited on Anodic Aluminum Oxide (AAO, pore size of 20 nm, Whatman), dried, and then observed using SEM. Figure 2b illustrates that the lateral size of the thin FG nanosheets is approximately 1-2 µm, indicating the successful exfoliation of fluorinated graphite flakes into 2D FG nanosheets. The FG supernatant was collected, filtered, and dried to obtain FG powder. The yield of the exfoliation process was measured at 31%. Additionally, ANF was prepared using a proton donor-assisted deprotonation method. Kevlar fibers, with a diameter of roughly 10 µm, were treated in a DMSO/KOH solution to weaken the hydrogen bonding between poly(p-phenylene terephthalamide) chains, resulting in the formation of nanofibers, as shown in Figure 2d.

3.2. Crystalline structure

XRD analysis was conducted to examine the crystalline structure of both fluorinated graphite and FG and ANF, as shown in Figure 3. The XRD pattern of fluorinated graphite exhibited a broad diffraction peak of 2θ at approximately 13.6°, as well as a strong and narrow peak at around 26.5°. The former peak corresponds to the (001) reflection, indicating the presence of a highly fluorinated hexagonal structure in graphene [14]. The latter peak is attributed to the (002) diffraction of the graphite structure, indicating good crystallinity [14]. The most notable distinction between fluorinated graphite and FG is the absence of the diffraction peak at 2θ = 26.5°, corresponding to a d-spacing of 3.34 Å. This disappearance indicates the successful exfoliation of fluorinated graphite sheets, resulting in the formation of thin-layered structures similar to the transformation from graphite to graphene [15]. Meanwhile, XRD of ANF shows two broad peaks located at 2θ of 14° and 20° which are corresponded to planes (110) and (200), respectively. The broad peaks indicate the amorphous properties of ANF.

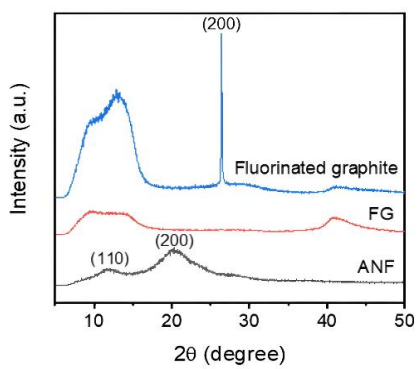

Figure 3. *XRD of fluorinated graphite, FG, and ANF*

3.3. Chemical bonding

Figure 4 illustrates the FT-IR spectra of fluorinated graphite, fluorinated graphene, and ANF. In the FT-IR spectrum of fluorinated graphite, two distinct peaks are noticeable at approximately 1245 cm^{-1} and 1300 cm^{-1}, which can be attributed to the C-F and C-F_2 bonds [16]. Following the exfoliation process, fluorinated graphene (FG) still exhibits two fluorination-related bonds, along with the emergence of a new peak centered at 3400 cm^{-1}, which is associated with hydroxyl (-OH) groups. The FT-IR spectrum of ANF shows various peaks in the wavenumber range of 600-1700 cm^{-1}, corresponding to oxygen-functional groups (-OH, -COOH, -COC) and carbon groups (C=C, C-C) [17]. Notably, a sharp peak at 3400 cm^{-1} related to amine (-NH_2) groups is present. It is anticipated that the amine groups can form hydrogen bonds with the hydroxyl groups on the surface of FG, which would contribute to the enhanced mechanical properties and thermal conductivity of the material.

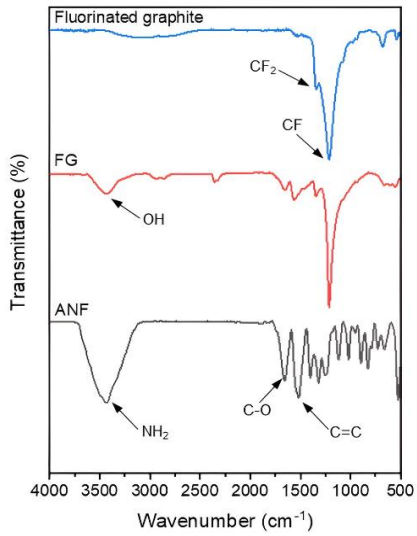

Figure 4. *FT-IR spectra of fluorinated graphite, FG, and ANF*

3.4. Mechanical properties

The mechanical properties of thermally conductive materials are crucial for their application in thermal management. Figure 5a displays the stress-strain curves of the FG/ANF films with varying FG content. The toughness values are summarized in Figure 5b.

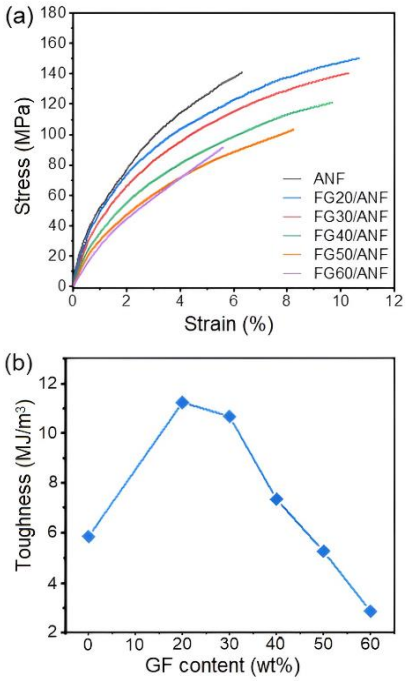

Figure 5. *Mechanical properties of the FG/ANF films: (a) stress-strain curves and (b) toughness*

The pure ANF film showed a high tensile strength of 141 MPa and an elongation at a break of 6.5%. When FG

was added, there was a slight decrease in tensile strength for the FG/ANF films. However, even with a high FG content of 40 wt%, the FG/ANF films maintained a substantial tensile strength of up to 111.7 MPa. For comparison, ANF films with 40 wt% boron nitride nanosheets (BNNS) had a modest tensile strength of only 70.9 MPa. This underscores the superior mechanical strength of the FG/ANF films compared to BNNS/ANF films, which can be attributed to the higher surface activity of FG, facilitated by the presence of hydroxyl groups. Importantly, the FG/ANF films also exhibited increased elongation at break compared to the pure ANF film. Furthermore, the FG30/ANF films showed a significant improvement in toughness, with a maximum increase of 88% compared to the pure ANF film, indicating enhanced tensile ductility. These excellent mechanical properties can be attributed to the well-arranged layered architecture and the formation of hydrogen bonding interactions between FG and ANFs in the FG/ANF films.

3.5. Thermal conductivity

The thermal conductivities (TC) in both in-plane ($\lambda_{//}$) and through-plane ($\lambda_{\perp}$) directions of FG/ANF films with different amounts of FG were determined using the laser flash method, as demonstrated in Figure 6a. The in-plane thermal conductivity of the pure ANF film was measured at 1.72 W/mK, primarily due to its high crystallization and the strong orientation of ANFs along the in-plane direction. Incorporating FG into the ANFs matrix led to a significant increase in in-plane thermal conductivity. For instance, the $\lambda_{//}$ of the FG10/ANF film containing 10 wt% FG content was 2.92 W/mK, which further rose to 5.73 W/mK for the FG30/ANF film. Notably, the film with 60 wt% FG/ANF displayed an outstanding $\lambda_{//}$ value of 25.11 W/mK, roughly 15 times higher than that of the pure ANF film. Additionally, the $\lambda_{\perp}$ of the FG/ANF films exhibited gradual enhancement with increasing FG content but remained noticeably lower than the corresponding $\lambda_{//}$ at the same FG content. This indicates a highly anisotropic thermal conduction behavior in the FG/ANF films. For example, the $\lambda_{\perp}$ of the pure ANF film was approximately 0.2 W/mK, which increased to only about 2 W/mK even with a substantial 60 wt% of FG. The superior $\lambda_{//}$ and the significant thermal conductivity anisotropy of the FG/ANF films can be attributed to the combined effects of the large intrinsic thermal conductivity anisotropy of FG and the well-ordered arrangement of FG within the ANF matrix along the in-plane direction.

The capacity to maintain thermal stability at high temperatures is a crucial factor for thermally conductive materials utilized in the thermal management of high-power integrated electronic devices. This specifically pertains to the findings illustrated in Figure 6b, which depict the relationship between temperature and the in-plane thermal conductivity ($\lambda_{//}$) of the FG40/ANF film comprising 40 wt% FG. According to the data presented, the FG40/ANF film exhibited exceptional thermal stability even at elevated temperatures. As the temperature increased up to 200°C, the $\lambda_{//}$ experienced only a slight decrease, less than a 10% reduction, indicating that its excellent thermal conductivity properties were maintained. Furthermore, Figure 6c portrays the relationship between the $\lambda_{//}$ of the FG40/ANF film and the number of bending cycles. The results demonstrate that the film's $\lambda_{//}$ remained largely unaffected even after subjecting it to 2000 bending cycles with a radius of curvature of 4 mm. The ability of the FG40/ANF film to preserve its thermal conductivity even after a substantial number of bending cycles is of great significance. This implies that the film can endure repeated mechanical stress without experiencing significant degradation in its thermal performance. Such a characteristic is pivotal in applications where flexibility and durability are prerequisites, such as in flexible electronic devices or wearable technology. These findings underscore that the film exhibits a high tolerance to elevated temperatures, reinforcing its reliability for thermal management applications. Figure 6d shows the comparison of thermal conductivity and tensile strength of FG60/ANF with composite films using various nanomaterials such as silver nanowires, MXene, reduced graphene oxide, and boron nitride nanosheet [19 - 24]. It is obvious that FG/ANF film shows greater values in both in-plane thermal conductivity and mechanical strength exceeding that of most reported nanofiber composites.

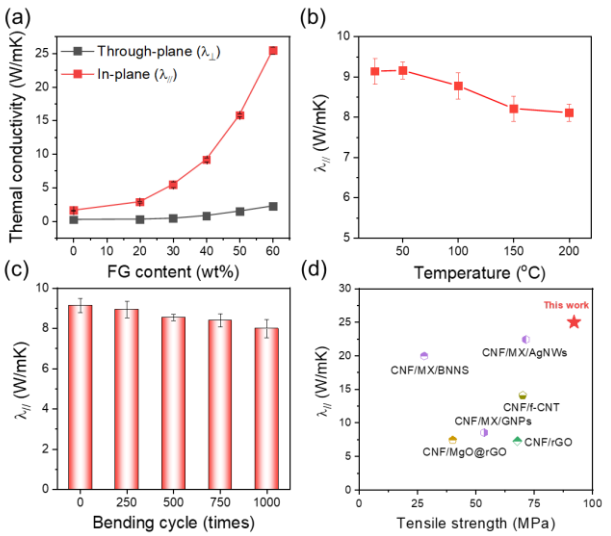

Figure 6. *(a) In-plane ($\lambda_{\perp}$) and through-plane ($\lambda_{//}$) thermal conductivity of FG/ANF films as a function of FG contents, (b) $\lambda_{//}$ of FG40/ANF film as a function of temperatures, (c) $\lambda_{//}$ of FG40/ANF film as a function of bending cycles, and (d) comparison on thermal conductivity vs tensile strength of the FG60/ANF film with composite films in previous reports, CNF: cellulose nano fibers, MX: $Ti_3C_2T_x$ MXene, BNNS: boron nitride nanosheets, AgNWs: silver nanowires, f-CNT: fluorinated carbon nanotubes, GNPs: graphene nanoplatelets, rGO: reduced graphene oxide, MgO: manganese oxide*

3.6. Volume electrical resistivity

In addition to having exceptional mechanical properties and high thermal conductivity, thermally conductive materials must also demonstrate effective electrical insulation performance to be effectively utilized in electronics. Figure 7 illustrates the relationship between the volume resistivity of the FG/ANF films and their FG content. It was observed that the volume of electrical resistivity slightly decreased with an increase in FG content. However, even at a substantial FG content of 40 wt%, the FG40/ANF film still maintained impressive electrical insulation performance, with a volume electrical

resistivity of approximately 2×10^{11} Ω·cm. Significantly, this value exceeded the critical resistivity threshold (109 Ω·cm) required to ensure effective electrical insulation. The combination of outstanding in-plane thermal conductivity and excellent electrical insulation properties in the FG/ANF films makes them highly promising for thermal management in high-power electronic devices. These films have the capability to efficiently conduct heat while maintaining sufficient electrical insulation, meeting the essential requirements for the reliable and safe operation of electronic components.

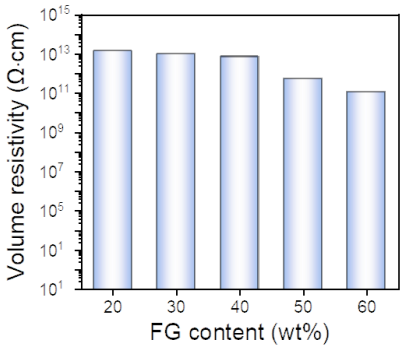

Figure 7. *Volume resistivity of the FG/ANF as a function of FG content*

4. Conclusions

We have successfully demonstrated the creation of flexible films with strong thermal conductivity, offering significant potential for thermal management purposes. These films were produced by combining 2D graphene flakes with 1D carbon nanofibers through a straightforward vacuum filtration process. The FG40/ANF films exhibited remarkable attributes, including a high in-plane thermal conductivity of 9.2 W/mK, excellent electrical insulation (with a volume resistivity exceeding 10^{11} Ω·cm), impressive tensile strength surpassing 110 MPa, and exceptional thermostability, maintaining their integrity at temperatures as high as 200°C. Furthermore, these films displayed exceptional durability by enduring 1000 folding cycles without any noticeable reduction in their in-plane thermal conductivity. We believe that these FG/ANF films are exceptionally well-suited for thermal management applications in a wide range of fields where both high-temperature stability and mechanical performance are essential.

Acknowledgements. This research is funded by Funds for Science and Technology Development of the University of Danang under project number B2021-DN02-04.

REFERENCES

[1] Q. W. Yan *et al.*, "Ultrahigh-aspect-ratio boron nitride nanosheets leading to superhigh in-plane thermal conductivity of foldable heat spreader", *Acs Nano*, vol. 15, no. 4, pp. 6489-6498, 2021.

[2] M. C. Vu, I. H. Kim, W. K. Choi, C. S. Lim, M. A. Islam, and S. R. Kim, "Highly flexible graphene derivative hybrid film: an outstanding nonflammable thermally conductive yet electrically insulating material for efficient thermal management", *ACS Appl Mater Interfaces*, vol. 12, no. 23, pp. 26413–26423, 2020.

[3] Y. Chen *et al.*, "Thermally conductive but electrically insulating polybenzazole nanofiber/boron nitride nanosheets nanocomposite paper for heat dissipation of 5g base stations and transformers", *ACS Nano*, vol. 16, no. 9, pp. 14323–14333, 2022.

[4] M. C. Vu *et al.*, "Ultrathin thermally conductive yet electrically insulating exfoliated graphene fluoride film for high performance heat dissipation", *Carbon*, vol. 157, pp. 741–749, 2020.

[5] Y. Guo, H. Qiu, K. Ruan, S. Wang, Y. Zhang, and J. Gu, "Flexible and insulating silicone rubber composites with sandwich structure for thermal management and electromagnetic interference shielding", *Composites Science and Technology*, vol. 219, 109253, 2022.

[6] J. Wang *et al.*, "Ultra-high electrical conductivity in filler-free polymeric hydrogels toward thermoelectrics and electromagnetic interference shielding", *Advanced Materials*, vol. 34, no. 12, 2109904, 2022.

[7] F. Kargar, Z. Barani, M. Balinskiy, A.S. Magana, J.S. Lewis, and A.A. Balandin, "Dual-functional graphene composites for electromagnetic shielding and thermal management", *Advanced Electronic Material*, vol. 5, no. 1, 1800558, 2019.

[8] M. C. Vu *et al.*, "Pressure-sensitive adhesive composites with a hydrophobic form of graphene oxide for enhanced thermal conductivity", *Macromolecular Research*, vol. 24, pp.1070–1076, 2016.

[9] M. C. Vu *et al.*, "Scalable ultrarobust thermoconductive nonflammable bioinspired papers of graphene nanoplatelet crosslinked aramid nanofibers for thermal management and electromagnetic shielding", *Journal of Materials Chemistry A*, vol. 9, no. 13, pp. 8527–8540, 2016.

[10] M. C. Vu *et al.*, "Scalable graphene fluoride sandwiched aramid nanofiber paper with superior high-temperature capacitive energy storage", *Chemical Engineering Journal*, vol. 444, 136504, 2022.

[11] R. Zbořil *et al.*, "Graphene fluoride: A stable stoichiometric graphene derivative and its chemical conversion to graphene", *Small*, vol. 6, no. 24, pp. 2885–2891, 2010.

[12] D. Mani *et al.*, "3D structured graphene fluoride-based epoxy composites with high thermal conductivity and electrical insulation", *Composites Part A: Applied Science and Manufacturing*, vol. 149, p. 106585, 2021.

[13] M. C. Vu *et al.*, "Nacre-inspired nanocomposite papers of graphene fluoride integrated 3D aramid nanofibers towards heat-dissipating applications", *Chemical Engineering Journal*, vol. 429, p. 132182, 2022.

[14] E. D. Grayfer *et al.*, "Synthesis, properties, and dispersion of few-layer graphene fluoride", *Chemistry–An Asian Journal*, vol. 8, no. 9, pp. 2015–2022, 2013.

[15] R. Stine, W. K. Lee, K. E. Whitener, J. T. Robinson, and P. E. Sheehan, "Chemical stability of graphene fluoride produced by exposure to XeF_2", *Nano letters*, vol. 13, no. 9, pp. 4311–4316, 2013.

[16] R. Zbořil *et al.*, "Graphene fluoride: A stable stoichiometric graphene derivative and its chemical conversion to graphene", *Small*, vol. 6, no. 24, pp. 2885–2891, 2010.

[17] B. Yang, L. Wang, M. Zhang, J. Luo, and X. Ding, "Timesaving, high-efficiency approaches to fabricate aramid nanofibers", *ACS Nano*, vol. 13, no. 7, pp. 7886–7897, 2019.

[18] Y. Wang, S. Xia, G. Xiao, J. Di, and J. Wang, "High-loading boron nitride-based bio-inspired paper with plastic-like ductility and metal-like thermal conductivity", *ACS applied materials & interfaces*, vol. 12, no. 11, pp. 13156–13164, 2020.

[19] E. Jiao *et al.*, "Robust Bioinspired MXene-Based Flexible Films with Excellent Thermal Conductivity and Photothermal Properties", *Compos Part A Appl Sci Manuf*, vol. 143, 106290, 2021.

[20] Q. Chu *et al.*, "Cellulose Nanofiber/Graphene Nanoplatelet/MXene Nanocomposites for Enhanced Electromagnetic Shielding and High In-Plane Thermal Conductivity", *ACS Appl Nano Mater*, vol. 5, no. 5, pp. 7217–7227, 2022.

[21] Y. Shang *et al.*, "Sandwiched Cellulose Nanofiber /Boron Nitride Nanosheet /Ti3C2Tx MXene Composite Film with High Electromagnetic Shielding and Thermal Conductivity yet Insulation Performance", *Compos Sci Technol*, vol. 214, 108974, 2021.

[22] M. Ma *et al.*, "Nanofibrillated Cellulose/MgO@rGO Composite Films with Highly Anisotropic Thermal Conductivity and Electrical Insulation", *Chemical Engineering Journal*, vol. 392, 123714, 2020.

[23] G. Li *et al.*, "Fabrication of Robust and Highly Thermally Conductive Nanofibrillated Cellulose/Graphite Nanoplatelets Composite Papers", *Compos Sci Technol*, vol. 138, pp. 179–185, 2017.

[24] X. Wang and P. Wu, "Fluorinated Carbon Nanotube/Nanofibrillated Cellulose Composite Film with Enhanced Toughness, Superior Thermal Conductivity, and Electrical Insulation", *ACS Appl Mater Interfaces*, vol. 10, no. 40, pp. 34311–34321, 2018.